



HAL
open science

Electrodeposition of MnO₂ on spray-coated nanostructured carbon framework as high performance material for energy storage

Clémence Rogier, Grégory Pognon, Paolo Bondavalli, Christophe Galindo, Giao Tran Minh Nguyen, Cédric Vancaeyzeele, Pierre-Henri Aubert

► To cite this version:

Clémence Rogier, Grégory Pognon, Paolo Bondavalli, Christophe Galindo, Giao Tran Minh Nguyen, et al.. Electrodeposition of MnO₂ on spray-coated nanostructured carbon framework as high performance material for energy storage. *Surface and Coatings Technology*, 2020, 384, pp.125310 -. 10.1016/j.surfcoat.2019.125310 . hal-03489742

HAL Id: hal-03489742

<https://hal.science/hal-03489742>

Submitted on 21 Jul 2022

HAL is a multi-disciplinary open access archive for the deposit and dissemination of scientific research documents, whether they are published or not. The documents may come from teaching and research institutions in France or abroad, or from public or private research centers.

L'archive ouverte pluridisciplinaire **HAL**, est destinée au dépôt et à la diffusion de documents scientifiques de niveau recherche, publiés ou non, émanant des établissements d'enseignement et de recherche français ou étrangers, des laboratoires publics ou privés.



Distributed under a Creative Commons Attribution - NonCommercial 4.0 International License

Electrodeposition of MnO₂ on spray-coated nanostructured carbon framework as high performance material for energy storage

Clémence Rogier^{1,2,*}, Grégory Pognon¹, Paolo Bondavalli¹, Christophe Galindo¹, Giao Tran Minh Nguyen², Cédric Vancaeyzeele², Pierre-Henri Aubert²

¹*Thales Research & Technology, 1 avenue Augustin Fresnel, 91767, Palaiseau, France*

²*Laboratoire de Physicochimie des Polymères et des Interfaces (EA 2528), Université de Cergy-Pontoise, 5 mail Gay-Lussac, 95031 Cergy-Pontoise Cedex, France*

**corresponding author, clemence.rogier@thalesgroup.com, +33 6 76 30 41 28*

Keywords

Spray coating

Electrodeposition

Nanostructured composite

Supercapacitor

Abstract

Carbon nanotubes/graphene/manganese dioxide nanostructured thin films are developed as supercapacitors electrodes in this contribution. The effects of nanostructuration and pseudocapacitance on electrochemical performances are investigated. The challenge is to assemble these materials in a composite electrode achieving controlled homogeneity, morphology, and composition. Mixing carbon nanotubes (CNTs) and graphene sheets in a hierarchical organization can increase the accessibility of the electrolyte to the entire active surface by creating a controlled porous network inside the electrode. The carbon nanomaterials are deposited on a current collector by dynamic spray gun deposition, an easily scalable, reproducible and industrially suitable method used for nano-structuration of thin films. MnO₂ nanocrystals are obtained by anodic electrodeposition directly on this conductive

nanostructured carbon framework. This binder free electrode is characterized by SEM, TEM, XPS, XRD, microporosity, Raman spectroscopy, and electrochemistry. Results show that the specific capacitance of the samples can reach 209 F/g thanks to a strong control of the MnO₂ morphology, particle size and to adequate Mn/C ratios. The electrode has very good stability with capacitance retention of 96% after 3 000 charge/discharge cycles.

1. Introduction

Supercapacitors are energy storage devices mainly used as complementary systems to batteries [1]. Their main characteristics are high power densities, very long cycle life and fast charge/discharge rates. Two types of supercapacitors can be identified in regard to their electrochemical mechanisms: electrochemical double-layer capacitors (EDLCs) and pseudocapacitors. EDLCs present carbon based materials as electrodes and their charges are electrostatically stored on the electrode surface in what is commonly defined as the double layer [2]. Pseudocapacitors possess redox active materials as electrodes and store energy through reversible faradaic reactions [3]. Many studies focus on increasing energy densities in supercapacitors while retaining high power densities, and in that regard pseudocapacitive materials, and most especially transition metal oxides, have been known to generate much higher capacitance and energy densities than EDLCs [4].

RuO_2 , MnO_2 , or NiO for example are suitable metal oxides for the positive electrode of a supercapacitor and Fe_2O_3 , V_2O_5 , or MoO_3 for its negative electrode [5]. Among these redox active materials MnO_2 is a promising candidate for the positive electrode with renewing interest from researchers in the last few years [6-9]. It is particularly attractive compared to other metal oxides for four main reasons (i) a large potential window in aqueous electrolyte ($\sim 1\text{V}$ versus $\sim 0,5\text{V}$ for NiO) (ii) the ability to function in neutral electrolytes preventing possible corrosion of packaging and collectors (iii) a low cost (unlike RuO_2), an abundant and environment friendly nature important for industry (iv) a high theoretical specific capacitance of $\sim 1370\text{ F/g}$ based on one-electron reaction per Mn atom [8,9]. However its low conductivity (10^{-1} à 10^{-5} S/m) [10] leads to pseudocapacitors with limited charge/discharge rate and therefore leads to low power densities.

In recent years, hybrid asymmetric supercapacitors have been studied to obtain high energy densities while maintaining high power densities and good cycle life stability [6,7] by combining EDLCs and pseudocapacitive materials in the same system and/or in the same

electrode. The strategy of our paper is to combine, within a specific architecture, carbon nanomaterials (association of graphene and carbon nanotubes i.e. CNTs) and manganese dioxide to achieve a hybrid positive electrode. The objective is to merge the faradaic behavior of the MnO_2 material with the electrostatic behavior of graphene and CNTs. In the last years, many studies on graphene derivatives have focused on exploiting the outstanding electrical properties of graphene sheets on a larger scale as well (graphene oxide [11], graphene-based composites [12]). Graphene is well known for its high theoretical surface area (up to $2630 \text{ m}^2/\text{g}$) and CNTs for their high conductivity in the longitudinal axis ($>10^6 \text{ S/m}$) [13]. It has been demonstrated in different papers [14, 15] that mixing these two materials allows to exploit the surface of graphene in a better way using the CNTs as spacers to avoid the restacking of the graphene layers, rendering the final structure more accessible to ions.

In this case, we combine the high potential capacitance of MnO_2 and the high conductivity of carbon nanomaterials to create a synergetic effect and generate higher electrochemical performances compared to pristine materials thanks to their optimized association [8,16]. The final electrode material combining MnO_2 with a high surface area conductive scaffold as shown in Fig. 1 should be the most promising architecture to enhance performances. Combinations of MnO_2 with carbon materials to form hybrid electrodes have been reported in the literature, for example with CNTs [17], graphene [18,19], activated carbon [20], or carbon aerogel [21]. Electrode specific capacitance, greatly influenced by mass loading, thickness of the electrode, and scan rate [9], can range from 150 to 300 F/g when mass of both carbon and metal oxide are taken into account. The originality of our approach compared to the literature relies on the association of CNTs and graphene before coating with the non-conductive MnO_2 . The increase of electrode resistance due to the metal oxide [22] will be limited considering that we preliminary created the conductive scaffold using graphene/CNTs mixtures and then covered it with the metal oxide. With better electronic conductivity, rate capability of the electrode will increase [3].

As previously published, these scaffolds have been fabricated exploiting an automated dynamic spray gun deposition [14]. This thin film deposition method generates homogeneous mats with finely tunable thickness. The structuration of the nanomaterials is reproducible, easily scalable and low-cost considering that it is compatible with large surfaces fabrication. Both anodic [23] and cathodic [24] electrodeposition can be used for MnO₂ coatings for supercapacitors with many different results depending on the conditions however there is still uncertainty upon which is the best method [25]. Galvanostatic anodic electrodeposition was chosen in this study for MnO₂ coatings because of its versatility and good controllability [26].

The aim of this manuscript is to present the optimization of a positive electrode material for asymmetric pseudocapacitors with high energy density. The electrode combines MnO₂, CNTs and graphene in an organized porous material, with MnO₂ deposited onto a pre-organized graphene/CNTs conductive scaffold. MnO₂ deposition conditions are studied in order to control the morphology of the material and tune the electrochemical performances.

2. Experimental section

2.1. Preparation of the nanostructured carbon electrode

Graphene oxide (i.e. GO, supplier Graphenea) and multi-walled carbon nanotubes (i.e. MWCNTs, supplier Sigma-aldrich) are dispersed in isopropanol at 0.5 g/L with a mass ratio of 50:50. It undergoes sonication for 24h using mild bath before deposition by dynamic spray gun on graphite current collectors heated at 120°C to obtain the GO-CNTs thin film. Electrochemical reduction is performed in LiNO₃ 0.5M for 5 min at -1.1V vs Ag/AgCl to obtain rGO-CNTs (r stands for reduced graphene oxide, i.e. rGO). The same procedure is applied to obtain rGO thin film without adding MWCNTs in the dispersion. The CNTs thin film is obtained without adding GO in the dispersion and without the step of electrochemical reduction. Electrode thicknesses are around 20 μm and carbon mass loadings range from 0.4 to 0.6 mg/cm².

2.2. Electrodeposition of manganese dioxide

Manganese dioxide is obtained by anodic electrodeposition on the rGO-CNTs thin film in $\text{MnSO}_4/\text{H}_2\text{SO}_4$ 0.1M at current densities between 2 and 32 mA/cm^2 . Deposition is either continuous or pulsed 0.1/1s ON/OFF. Electrodes are then rinsed with water and dried under vacuum before characterization. Same procedure applies for CNTs- MnO_2 and rGO- MnO_2 hybrid thin films. Electrode thicknesses are around 20-30 μm and final electrodes weight 1-1.5 mg/cm^2 (total mass of active material: carbon and MnO_2). Samples are weighed before and after electrodeposition with a Sartorius microbalance (precision 0,001 mg) to determine MnO_2 mass loading and MnO_2/C ratios are confirmed by thermogravimetric analysis (TGA) with a Thermofischer instrument.

2.3. Characterization of the materials

Morphologies of the electrodes are characterized by scanning electron microscopy (i.e. SEM, Zeiss Gemini). Surfaces of the samples are observed, as well as cross sections obtained under Focused Ion Beam (i.e. FIB, Gallium ions). N_2 adsorption isotherms measurements are performed using a Quantachrome Autosorb instrument at 77K. Specific surface areas are calculated with the Brunauer-Emmett-Teller (BET) theory, and pore size distribution is calculated with the DFT method. Chemical states of the electrodes are studied by X-ray photoelectron spectroscopy (i.e. XPS, Kratos Axis Ultra) and Raman spectroscopy (Renishaw Raman microscope). Conductivity measurements are obtained by Hall Effect (HMS5500 Ecopia system). Crystallinity is characterized by X-ray diffraction (i.e. XRD, Pananalytical).

2.4. Electrochemical performances

Electrochemical characterizations are performed with a Biologic VMP300 workstation. Samples are tested as working electrodes in a 3-electrodes configuration vs Ag/AgCl and with a platinum counter electrode in Na_2SO_4 1M. Cyclic voltammetry (CV) curves are obtained with scan rates from 2 to 200 mV/s and a potential window of 0-0.9V.

Gravimetric capacitance ($F.g^{-1}$) is calculated from CV curves by the mass of active material (carbon and MnO_2). Electrochemical impedance spectroscopy (EIS) is performed between 5 mHz and 200 kHz with an amplitude of 10 mV around 0.45V (OCP).

3. Results and discussion

Dynamic spray gun deposition is used to obtain a nanostructured GO-CNTs thin film, then electrochemical reduction of GO is performed according to the literature [27] to increase electronical conductivity of the carbon structure from 2690 S/m (GO-CNTs) to 3620 S/m (rGO-CNTs). Then Mn^{2+} ions in solution are oxidized into MnO_2 with the application of a current density in acidic conditions [28] on this carbon matrix to form rGO-CNTs- MnO_2 .

Crystallinity of the manganese oxide was studied by X-ray diffraction after deposition on a platinum grid as shown in Fig. 2a. The samples show very poor crystallinity. Two diffraction peaks are nonetheless observed at 37° and 66° and may be attributed to the cryptomelane phase (JCPDS 44-0141) [29]. Raman spectroscopy shown in Fig. 2b was performed on the rGO-CNTs and rGO-CNTs- MnO_2 samples. After MnO_2 deposition, a peak at 640 cm^{-1} is observed due to Mn-O stretching symmetric vibration band characteristic of MnO_2 [30]. The typical D and G band of carbon are observed at 1349 cm^{-1} and 1578 cm^{-1} respectively [31] before and after MnO_2 deposition.

X-ray photoelectron spectroscopy was carried out to analyze oxidation states of the rGO-CNTs- MnO_2 composite material. The full-scan XPS spectrum shown in Fig. 2c reveals the existence of Mn, C, and O atoms in our sample. The C 1s, Mn 2p, and Mn 3s core-level spectra were then obtained at high resolution. The C 1s core level deconvoluted peak is shown in Fig. 2d. Peaks are observed at 284.4 and 284.9 eV and characterize C=C sp^2 and C-C sp^3 bonds respectively. Peaks for the remaining functional groups containing oxygen are also observed at 286.3 eV (C-O), 288.2 eV (C=O), and 290.7 (O-C=O) which is consistent with the literature on oxidized graphene [31]. GO was considered successfully reduced in rGO

after electrochemical treatment since O/C concentration ratio is only of 0.16. Oxidation state of the deposited manganese oxide was then investigated by analysis of the Mn 2p (Fig. 2e) and Mn 3s (Fig. 2f) spectra. The Mn 2p core-level shows the two peaks of Mn 2p_{1/2} and Mn 2p_{3/2} at 653.7 and 641.9 eV respectively and an energy separation of 11.8 eV. These results are in agreement with the XPS characteristics of MnO₂ as presented by Biesinger et al. [32] and observed since in the literature [6,29,33]. The Mn oxidation state can be further determined with the Mn 3s core-level spectrum which shows a peak splitting of 5.0 eV between 89.1 and 84.1 eV. The value of this peak separation is directly correlated to the oxidation state of the manganese and peak separation values were reported in the literature as 6.0, 5.4 and 4.7 eV for Mn²⁺, Mn³⁺ and Mn⁴⁺ respectively [32]. In addition, it was previously shown that a linear relation exists between the peak separation and the oxidation state of the manganese [34]. Therefore the MnO₂ compound deposited in our rGO-CNTs-MnO₂ structure has a mean oxidation state of 3.6 and a mixed valence of Mn³⁺ and Mn⁴⁺.

The morphologies of the electrodes were studied by scanning electron microscopy. Manganese oxide deposited on rGO-CNTs by continuous electrodeposition (CE) leads to cover the top of the sample with MnO₂ grains of 1 to 5 μm as seen in Fig. 3a. A blocking layer [35] is built up on the top of the carbon samples when deposition time increases and Mn²⁺ ions are not able to fully penetrate the rGO-CNTs matrix. Indeed, manganese dioxide remains at the surface of the electrode and stops the formation of a homogeneous composite material through the whole thickness of the electrode. A sample prepared via pulsed electrodeposition (PE) is shown in Fig. 3b. The current is applied with pulses of 0.1 s (ON) and resting times between current pulses of 1 s (OFF). In this case, the metal oxide is finely deposited as nanoparticles on the surface of the carbon nanomaterials instead of forming a blocking continuous layer. Images of the cross-section of the sample were obtained by Focused Ion Beam technic. In this case, adding a resting time during the desposition allows the Mn²⁺ ions to diffuse through the layer of carbon and allows particles to grow inside the carbon matrix as

can be seen in Fig. 3d. However for a carbon thickness of 20 μm , MnO_2 nanoparticles penetrate only 8 μm with a gradient in particle size as observed in the cross section image in Fig. 3c. Resting time needs to be optimized to deposit metal oxide through the full layer, or carbon matrix thickness should be reduced below 8 μm in order to evaluate the best configuration, taking the maximum benefit of each contribution. The oxide grows on the CNTs and acts as a spacer as well preventing even more the restacking of the carbon architecture. At the bottom of the sample rGO-CNTs layers are very compact, whereas at the top of the sample rGO-CNTs- MnO_2 shows a less dense multilayer organisation. The nanoparticles of MnO_2 are inserted in between reduced graphene oxide layers in a hierarchical architecture to form a composite material. Such successful nanostructuring of the sample is important for the improvement of electrochemical performances [10].

Measurements of nitrogen adsorption isotherms were performed to study the porosity and accessibility into this composite material and are represented in Fig. 4a. BET surface areas and pore size distributions were calculated. Adsorption curves show type IV isotherms typical of mesoporous materials [36]. The rGO-CNTs carbon matrix shows a specific surface area of 259 m^2/g , and the rGO-CNTs- MnO_2 composite of 360 m^2/g (48% of MnO_2 mass loading). As observed in Fig. 4b, increase in surface area can be explained by the creation of a new type of pores (about 1-2 nm) after deposition of MnO_2 nanoparticles. Pore size distribution of the multilayered rGO-CNTs architecture is kept after deposition of the metal oxide. The insertion of manganese oxide nanoparticles does not impact the porous architecture of the carbon network. More MnO_2 redox active sites may be available for ions for charge storage with this high surface area electrode.

Deposition conditions have a great influence on electrochemical performances. Capacitance of various electrodes were calculated for CV at different scan rates (2, 20 and 200 mV/s) and summarized in Table 1. MnO_2 mass loading is determined by thermogravimetric analysis as can be seen in Fig. 5a for a 60% mass loading. As stated

previously, pulsed electrodeposition allows the performances and especially the rate capability to increase (higher capacitance at 200 mV/s) compared to continuous electrodeposition at the same current density (CE-2 mA/cm² versus PE-2 mA/cm²). Ion solid-state diffusion inside the crystalline structure of the cryptomelane is limited. Thanks to the nanostructuring, the amount of bulk MnO₂ which is not accessible to Na⁺ ions during charge storage mechanism decreases drastically [10]. The large MnO₂ surface provided by the formation of nanoparticles (diameters from 130 to 250 nm) should be favorable to exploit more electrochemically active charge transfer sites and thus enhance the capacitance and the rate capability.

MnO₂ particle size variation was also observed in scanning electron microscopy for pulsed depositions at different current densities and images are represented in Fig. 6. At 2 mA/cm², the nanoparticles have diameters around 250 nm and are constituted of nanopetals with thicknesses around 16 nm. At 32 mA/cm², these dimensions are nearly two orders of magnitude lower (~130 nm for the particles and ~7 nm for the petals). For a similar mass loading of manganese oxide (~55%) but with smaller nanoparticles, capacitance is higher (209 F/g for 130 nm instead of 138 F/g for 250 nm at 2 mV/s) confirming the importance of nanostructuring (see Table 1, PE-2 mA/cm² versus PE-32 mA/cm²). Finally, the influence of MnO₂ mass loading was studied for the same current density by tuning only the duration of MnO₂ deposition (see Table 1, PE-16 mA/cm² with 33%, 40% and 60% mass loading). At a slow scan rate, capacity increases with mass loading. However rate capability decreases for 60% of manganese oxide (67 F/g at 200 mV/s instead of 75 F/g for MnO₂ 40%). To optimize the performances, a compromise needs to be found for the amount of electrodeposited metal oxide: when the mass loading is too low, the increase in performances due to pseudocapacitance is limited however when the mass loading is too high, the conductivity of the electrode decreases (2398 S/m for 33% of MnO₂ and 1473 S/m for 60% of MnO₂) and the rate capability drops too. It can be noted that this conductivity values are very high for hybrid

materials containing manganese oxide thanks to the carbon scaffold. Fig. 5b represents capacitance versus MnO₂ mass loading at slow scan rates (2 mV/s) and at faster scan rates (200 mV/s) to illustrate that the optimized range for mass loading is situated between 40% and 60% of MnO₂.

CV curves at different scan rate of the optimized rGO-CNTs-MnO₂ sample (PE – 32 mA/cm² – 55% MnO₂) are shown in Fig. 7a. The total mass loading of this sample is 1.0 mg/cm². The rectangular shapes of the curves show a very good pseudocapacitive behavior. The curves are symmetrical. It points out the good reversibility of the redox reaction within the chosen potential window. Deviation from this rectangular shape at higher scan rates indicates the limit of pseudocapacitance in terms of rate capability. Capacitance of rGO-CNTs-MnO₂ is compared to rGO-CNTs, rGO-MnO₂ and CNTs-MnO₂ between 2 and 200 mV/s in Fig. 7b. Performances are higher after MnO₂ deposition even at high scan rates, which highlights the importance of the pseudocapacitive contribution. The positive influence of the multilayered organized rGO-CNTs scaffold is underlined as well by the increase in capacitance compared to MnO₂ deposited on a bare CNTs mat or a bare rGO mat. Both the CNTs-MnO₂ material (55% MnO₂ and total mass loading of 1.0 mg/cm²) and the rGO-MnO₂ material (50% MnO₂ and total mass loading of 1.2 mg/cm²) have a lower specific capacitance than the rGO-CNTs-MnO₂ association whatever the scan rate. This important gain in capacitance (20 to 30%) can be attributed to the improved accessibility to ions of the rGO-CNTs multilayered architecture for ions. The CNTs serve as spacers between the rGO sheets and their association builds up a conductive porous matrix that allows proper MnO₂ active sites available to ions for charge storage with a high surface area and appropriate porosity of 2 to 6 nm pores. The pores are well designed for the insertion of aqueous solvated ions (Mn²⁺ 0.49 nm, Na⁺ 0.33 nm) [37].

Electrochemical impedance spectroscopy was performed to study the frequency response of the electrode material. Nyquist diagrams of rGO-CNTs and rGO-CNTs-MnO₂ are

represented in Fig. 7c. Four domains can be distinguished in Nyquist [30]: 1) high frequency intersection with the real axis 2) high-to-mid-frequency semicircle 3) mid-frequency straight line at 45° to the real axis 4) low-frequency almost vertical line. The high frequency intercept is the same for both samples ($\sim 3\text{-}3.5 \Omega$). It represents a combination of ionic resistance of electrolyte, collector resistance and collector/material interface resistance. The semicircle is associated to charge transfer resistance at the electrode/electrolyte interface. In the case of the carbon structure before MnO_2 electrodeposition, the charge transfer resistance is due to remaining functional group on graphene. In the case of the pseudocapacitive material, it is also due to ion insertion in the MnO_2 lattice [30]. Charge transfer resistance is very low in both cases ($\sim 0.7 \Omega$) indicating fast kinetics and a good activity for MnO_2 thanks to the nanostructuration [33]. At low frequency, for rGO-CNTs, the straight line is closer to a vertical line compared to rGO-CNTs- MnO_2 . The carbon electrode is more steered by capacitive behaviors whereas there are still ion diffusion limitations at low frequency for the composite material. This is due to solid-state diffusion inside the MnO_2 lattice. At mid-frequency the typical Warburg resistance (45° slope) is due to ion diffusion processes in the pores of the electrode. Surprisingly, this Warburg slope is much less pronounced for the composite electrode compared to the carbon matrix one meaning better ion diffusion in the composite material. This result is very interesting and highlights a different behavior compared to what has been observed in the literature until now [13,30]. Electrochemical kinetics are in close relations with the porous morphology, the good conductivity and the interlayer spacing between graphene sheets [38]. This means the porosity is even more accessible to ions after MnO_2 deposition and correlates with the formation of porosity observed in isotherms analysis.

Galvanostatic charge-discharge studies at different current densities are represented in Fig. 8a for the rGO-CNTs- MnO_2 electrode material (PE – 16 mA/cm^2 – 60% MnO_2). They indicate a mostly capacitive nature for the composite electrode with nearly linear and

symmetric charge-discharge curves. Resistance of the material can be calculated from the IR drop at each current density and is found to be of 2.9Ω which is close to the value found in impedance spectroscopy in Fig. 7c. Specific capacitance of 124 F/g, 108 F/g and 75 F/g are calculated from discharge curves at 0.6 A/g, 5 A/g and 30 A/g with discharge times of 1.8 s, 18 s and 3 min respectively which indicate a good capacitance retention of 60% at high current density. The stability of this electrode was then evaluated by performing 3 000 cycles. The retention of capacitance through cycling and the 1st and 3000th CV curves at 20 mV/s are shown in Fig. 8b. Performances of our electrode material are compared to literature values in Table 2. 96% of the capacitance is conserved after 3 000 cycles demonstrating an outstanding electrochemical stability.

4. Conclusion

A hybrid nanostructured rGO-CNTs-MnO₂ electrode material was obtained combining dynamic spray gun and pulsed electrodeposition, two versatile and industrially suitable fabrication methods. The strategy of developing a new type of electrode with multilayered rGO-CNTs scaffold as a carbon matrix for metal oxide deposition give a clear asset in terms of electrochemical performances of pseudosupercapacitors. The rGO-CNTs multilayered structure provides a high specific surface area and an electrically conductive network; MnO₂ nanoparticles insure an effective faradaic behavior necessary to enhance capacitance. We have demonstrated that the deposition conditions play an important role on the morphology of the electrodes and thus on the electrochemical performances of the nanocomposite. In fact, measurements show that smaller MnO₂ nanoparticles can be obtained by tuning current density during the anodic deposition enhancing capacitance (149 F/ for 130 nm particles instead of 108 F/g for 250 nm particles at 20 mV/s). MnO₂ mass loading can be controlled as well and can improve rate capability. Final electrode has a capacitance of 209 F/g and a very good stability with capacitance retention of 96% after 3000 cycles. To enhance capacitance,

MnO₂ deposition in the carbon matrix needs to be further optimized to achieve a homogeneous material through all the cross section of the electrode.

Acknowledgements

The authors would like to acknowledge the financial support of the ANRT through the C. Rogier PhD thesis (CIFRE 2016/1436). The authors would also like to thank Jocelyne Leroy from the CEA Saclay for performing the XPS measurements.

Declarations of interest: none.

Bibliography

- [1] R. Kötz, M. Carlen, Principles and applications of electrochemical capacitors, *Electrochim. Acta* 45 (2000) 2483-2498.
- [2] A. Gonzalez, E. Goikolea, J. A. Barrena, R. Mysyk, Review on supercapacitors: Technologies and materials, *Renewable Sustainable Energy Rev.*, 58 (2016) 1189-1206.
- [3] J. Wang, S. Dong, B. Ding, Y. Wang, X. Hao, H. Dou, Y. Xia, X. Zhang, Pseudocapacitive materials for electrochemical capacitors: from rational synthesis to capacitance optimization, *National Sci. Rev.* 4 (2017) 71-90.
- [4] P. Simon, Y. Gogotsi, Materials for electrochemical capacitors, *Nat. Mater.* 7 (2008) 845-854.
- [5] F. Wang, S. Xiao, Y. Hou, C. Hu, L. Liu, Y. Wu, Electrode materials for aqueous asymmetric supercapacitors, *RSC Adv.* 3 (2013) 13059–13084.
- [6] Y. Liu, L. Guo, X. Teng, J. Wang, T. Hao, X. He, Z. Chen High-performance 2.5 V flexible aqueous asymmetric supercapacitors based on K⁺/Na⁺-inserted MnO₂ nanosheet, *Electrochimica Acta* 300 (2019) 9-17.
- [7] K. Li, X. Liu, T. Zheng, D. Jiang, Z. Zhou, C. Liu, X. Zhang, Y. Zhang, D. Losic, Tuning MnO₂ to FeOOH replicas with bio-template 3D morphology as electrodes for high performance asymmetric supercapacitors, *Chem. Eng. J.* 370 (2019) 136–147.
- [8] J.-G. Wang, F. Kang, B. Wei, Engineering of MnO₂-based nanocomposites for high-performance supercapacitors, *Prog. Mater. Sci.* 74 (2015) 51-124.
- [9] M. Huang, F. Li, F. Dong, Y. X. Zhang, L. L. Zhang, MnO₂-based nanostructures for high-performance supercapacitors, *J. Mater. Chem. A* 3 (2015) 21380-21423.
- [10] V. Augustyn, P. Simon, B. Dunn, Pseudocapacitive oxide materials for high-rate electrochemical energy storage, *Energy Environ. Sci.* 7 (2014) 1597-1614.
- [11] Q. Ke, J. Wang, Graphene-based materials for supercapacitor electrodes : A review, *J. Materiomics* 2 (2016) 37-54.
- [12] S. Stankovich, D.A. Dikin, G.H.B. Dommett, K.M. Kohlhaas, E.J. Zimney, E.A. Stach, R.D. Piner, S.B. T. Nguyen, R.S. Ruoff, Graphene-based composite materials, *Nature* 442 (2006) (7100): 282
- [13] L. L. Zhang, R. Zhou, X. S. Zhao, Graphene-based materials as supercapacitor electrodes, *J. Mater. Chem.* 20 (2010) 5983-5992.
- [14] C. Delfaure, P. Legagneux, D. Pribat, P. Bondavalli, Supercapacitor Electrode Based on Mixtures of Graphite and Carbon Nanotubes Deposited Using a Dynamic Air-Brush Deposition Technique, *J. Electrochem. Soc.* 160 (2013) A601-A606.

- [15] Q.Cheng, J.Tang, J.Ma, H.Zhang, N.Shinya, L.Qin, Graphene and carbon nanotube composite electrodes for supercapacitors with ultra-high energy density, *Phys. Chem. Chem. Phys.*, 13 (2011) 17615-17624
- [16] T.Bi, H.Fang, J.Jiang, X.He, X.Zhen, H.Yang, Z.Wei, Z.Jia, Enhance supercapacitive performance of MnO₂/3D carbon nanotubes-graphene as a binder-free electrode, *J. Alloys Compd* 787 (2019) 759-766.
- [17] L. Li, Z. A. Hu, N. An, Y. Y. Yang, Z. M. Li, H. Y. Wu, Facile Synthesis of MnO₂/CNTs Composite for Supercapacitor Electrodes with Long Cycle Stability, *J. Phys. Chem. C* 118 (2014) 22865-22872.
- [18] Z. Luan, Y. Tian, L. Gai, H. Jiang, X. Guo, Y. Yang, Environment-benign synthesis of rGO/MnO_x nanocomposites with superior electrochemical performance for supercapacitors, *J. Alloys Compd.*, 729 (2017) 9-18.
- [19] S. Deng, D. Sun, C. Wu, H. Wang, J. Liu, Y. Sun, H. Yan, Synthesis and electrochemical properties of MnO₂ nanorods/graphene composites for supercapacitor applications, *Electrochim. Acta* 111 (2013) 707-712.
- [20] R. Liu, E. Liu, R. Ding, K. Liu, Y. Teng, Z. Luo, Z. Li, T. Hu, T. Liu, Facile in-situ redox synthesis of hierarchical porous activated carbon@MnO₂ core/shell nanocomposite for supercapacitors, *Ceram. Int.* 41 (2015) 12734-12741.
- [21] H. Z. Chi, Y. Q. Wu, Y. K. Shen, C. Zhang, Q. Xiong, H. Qin, Electrodepositing manganese oxide into a graphene hydrogel to fabricate an asymmetric supercapacitor, *Electrochim. Acta* 289 (2018) 158-167.
- [22] H. Huang, W. Zhang, Y. Fu, X. Wang, Controlled growth of nanostructured MnO₂ on carbon nanotubes for high-performance electrochemical capacitors, *Electrochim. Acta* 152 (2015) 480-488.
- [23] N. R. Chodankar, S.H. Ji, D.H. Kim, Low-cost superior symmetric solid-state supercapacitors based on MWCNTs/MnO₂ nanocomposite thin film, *J. Taiwan Inst. Chem. Eng.* 80 (2017) 503-510.
- [24] Y. Wang, H. Liu, X. Sun, I. Zhitomirsky, Manganese dioxide carbon nanotube nanocomposites for electrodes of electrochemical supercapacitors, *Scr. Mater.* 61 (2009) 1079-1082.
- [25] C. P. Yi, S. R. Majid, The Electrochemical Performance of Deposited Manganese Oxide-Based Film as Electrode Material for Electrochemical Capacitor Application, in *Semiconductors: Growth and Characterization*, 2018.
- [26] M. Kazazi, Effect of electrodeposition current density on the morphological and pseudocapacitance characteristics of porous nano-spherical MnO₂ electrode, *Ceram. Int.* 44 (2018) 10863-10870.

- [27] S. Ghasemi, R. Hosseinzadeh, M. Jafari, MnO₂ nanoparticles decorated on electrophoretically deposited graphene nanosheets for high performance supercapacitor, *Int. J. Hydrogen Energy* 40 (2015) 1037-1046.
- [28] P. G. Perret, P. R. L. Malenfant, C. Bock, B. MacDougall, Electro-Deposition and Dissolution of MnO₂ on a Graphene Composite Electrode for Its Utilization in an Aqueous Based Hybrid Supercapacitor, *J. Electrochem. Soc.* 159 (2012) A1554-A1561.
- [29] M. Kim, Y. Hwang, J. Kim, Graphene/MnO₂-based composites reduced via different chemical agents for supercapacitors, *J. Power Sources* 239 (2013) 225-233.
- [30] Y. Liu, D. Yan, R. Zhuo, S. Li, Z. Wu, J. Wang, P. Ren, P. Yan, Z. Geng, Design, hydrothermal synthesis and electrochemical properties of porous birnessite-type manganese dioxide nanosheets on graphene as a hybrid material for supercapacitors, *J. Power Sources* 242 (2013) 78-85.
- [31] S. Pei, H.-M. Cheng, The reduction of graphene oxide, *Carbon* 50 (2012) 3210-3228.
- [32] M.C. Biesinger, B.P. Payne, A.P. Grosvenor, L.W.M. Lau, A.R. Gerson, R.S.C. Smart, Resolving surface chemical states in XPS analysis of first row transition metals, oxides and hydroxides: Cr, Mn, Fe, Co and Ni, *Applied Surface Science* 257 (2011) 2717-2730.
- [33] J. Wang, J.G. Wang, H. Liu, C. Wei, F. Kang, Zinc ion stabilized MnO₂ nanospheres for high capacity and long lifespan aqueous zinc-ion batteries, *J. Mater. Chem. A*, 7 (2019) 13727-13735
- [34] M. Toupin, T. Brousse, D. Bélanger, Charge Storage Mechanism of MnO₂ Electrode Used in Aqueous Electrochemical Capacitor, *Chem. Mater.* 16 (2004) 3184-3190.
- [35] M. Li, H. G. Park, Improved high-rate performance of a supercapacitor electrode from manganese-oxide-coated vertically aligned carbon nanotubes prepared by a pulsed current electrodeposition method, *Electrochim. Acta* 296 (2019) 676-682.
- [36] W. Qi, X. Li, Y. Wu, H. Zeng, C. Kuang, S. Zhou, S. Huang, Z. Yang, Flexible electrodes of MnO₂/CNTs composite for enhanced performance on supercapacitors, *Surf. Coat. Technol.* 320 (2017) 624-629.
- [37] Y. Marcus, Thermodynamics of solvation of ions. Part 5. Gibbs free energy of hydration at 298.15 K, *J. Chem. Soc., Faraday Trans.* 87 (1991) 2995-2999.
- [38] H. Sun, J.G. Wang, X. Zhang, C. Li, F. Liu, W. Zhu, W. Hua, Y. Li, M. Shao Nanoconfined Construction of MoS₂@C/MoS₂ Core-Sheath Nanowires for Superior Rate and Durable Li-Ion Energy Storage, *ACS Sustainable Chem. Eng.* 7 (2019) 5346-5354.

Table 1

Summary of MnO₂ mass loading, capacitance and MnO₂ nanoparticle size for different electrodeposition conditions (pulsed or continuous, variation in current density and deposition time)

Deposition conditions	MnO ₂ loading	C			Particle size
		(2 mV/s)	(20 mV/s)	(200 mV/s)	
CE-2 mA/cm ²	60%	135 F/g	97 F/g	60 F/g	~1-5 μm
PE-2 mA/cm ²	55%	138 F/g	104 F/g	69 F/g	~250 nm
PE-32 mA/cm ²	55%	209 F/g	149 F/g	83 F/g	~130 nm
PE-16 mA/cm ²	33%	127 F/g	97 F/g	66 F/g	~200 nm
PE-16 mA/cm ²	40%	154 F/g	112 F/g	75 F/g	~200 nm
PE-16 mA/cm ²	60%	161 F/g	115 F/g	67 F/g	~200 nm

CE: Continuous electrodeposition and PE: Pulsed electrodeposition

Table 2

Summary of MnO₂-based hybrid electrode materials for supercapacitors – Abbreviations: AC, Activated Carbon; Gr, Graphene, Electrodep., Electrodeposition; Decomp., Decomposition.

Electrode material	Synthesis	Loading (mg/cm ²)	C (F/g)	Scan rate (mV/s)	Stability	Ref.
AC/MnO ₂	Hydrothermal	3	193	2	77% 1500 cycles	[20]
rGO/MnO ₂	Hydrothermal	/	218	5	93% 1000 cycles	[19]
Gr/MnO ₂	Hydrothermal	6	237	10	87% 2000 cycles	[30]
CNT/MnO ₂	Redox	10	152	5	93% 5000 cycles	[22]
CNT/MnO ₂	Redox	/	140	10	95% 10000 cycles	[17]
CNT/Gr/MnO ₂	Thermal decomp.	0.5	365	20	97% 1000 cycles	[16]
rGO/MnO ₂	Electrodep.	0.13	270	20	87% 1200 cycles	[27]
CNT/MnO ₂	Electrodep.	0.62	125	100	87% 2000 cycles	[35]
rGO/CNT/MnO ₂	Electrodep.	1	209	2	96% 3000 cycles	This work

Fig. 1. Scheme of the structure

Graphene-CNTs-MnO₂ composite architecture

Fig. 2. Chemical state and structure characterization

(a) XRD pattern of MnO₂ electrodeposited on a Pt grid (b) Raman spectra of rGO-CNTs-MnO₂ and rGO-CNTs (c) XPS Mn2p spectrum of rGO-CNTs-MnO₂ and (d) XPS C1s spectrum of rGO-CNTs-MnO₂

Fig. 3. Morphology

SEM images of rGO-CNTs-MnO₂ (a) continuous electrodeposition top view (b) pulsed electrodeposition top view (c) pulsed electrodeposition FIB cross section at different magnifications

Fig. 4. Porosity

(a) N₂ adsorption-desorption isotherms and (b) pore size distribution for rGO-CNTs and rGO-CNTs-MnO₂

Fig. 5. Mass loading

(a) Thermogravimetric analysis of the rGO-CNTs-MnO₂ composite material for a 60% MnO₂ mass loading (b) Specific capacitance as a function of MnO₂ mass loading for PE-16 mA/cm²

Fig. 6. Particle size

SEM images of rGO-CNTs-MnO₂ with 55% MnO₂ mass loading for different deposition conditions (a,c) PE-2 mA/cm² (b,d) PE-32 mA/cm²

Fig. 7. Electrochemical characterization

Electrochemical performances of rGO-CNTs-MnO₂ (a) CV curves at different scan rates (2, 20 and 200 mV/s) (b) Gravimetric capacitance at different scan rates compared to rGO-CNTs, rGO-MnO₂ and CNTs-MnO₂ (c) cycle stability at 20 mV/s (d) EIS compared to rGO-CNTs

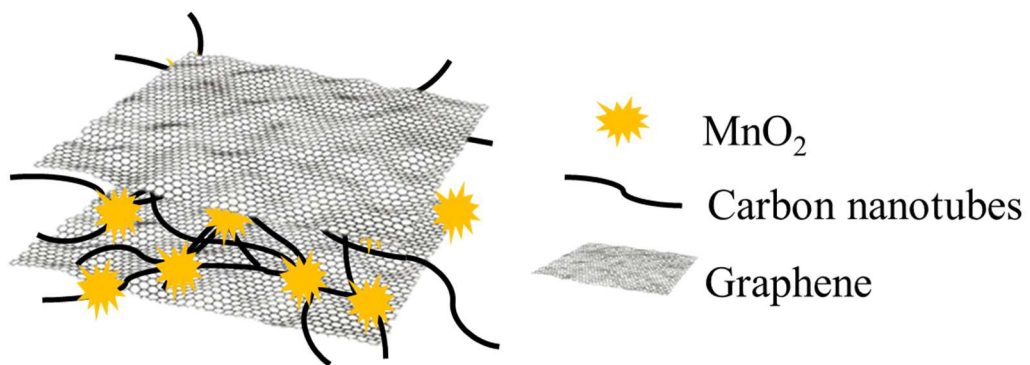


Fig. 1

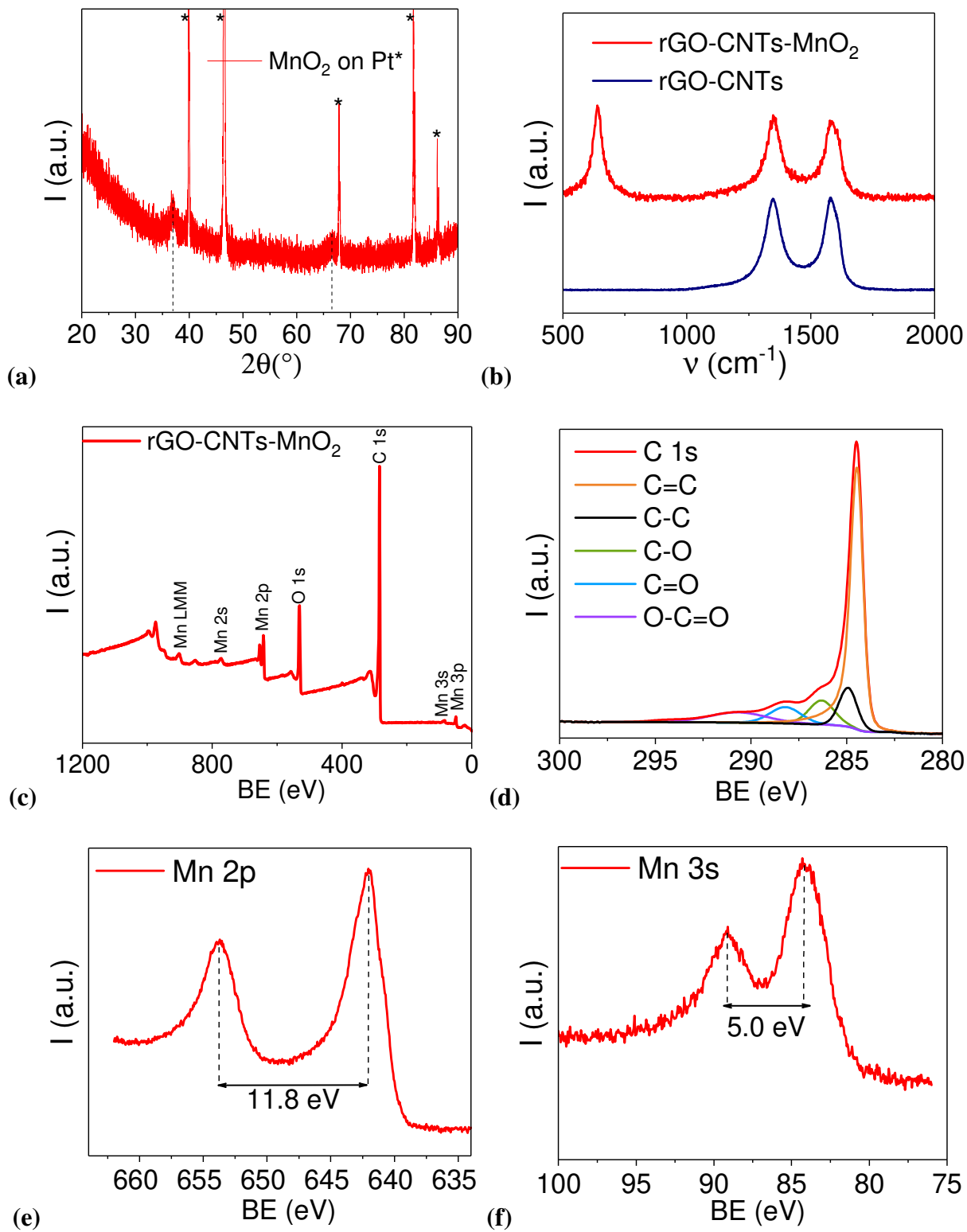


Fig. 2

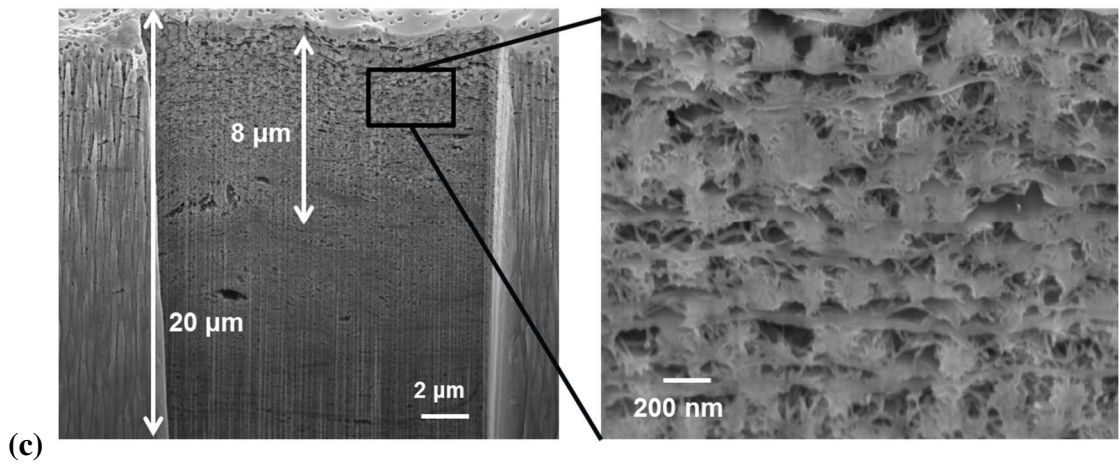
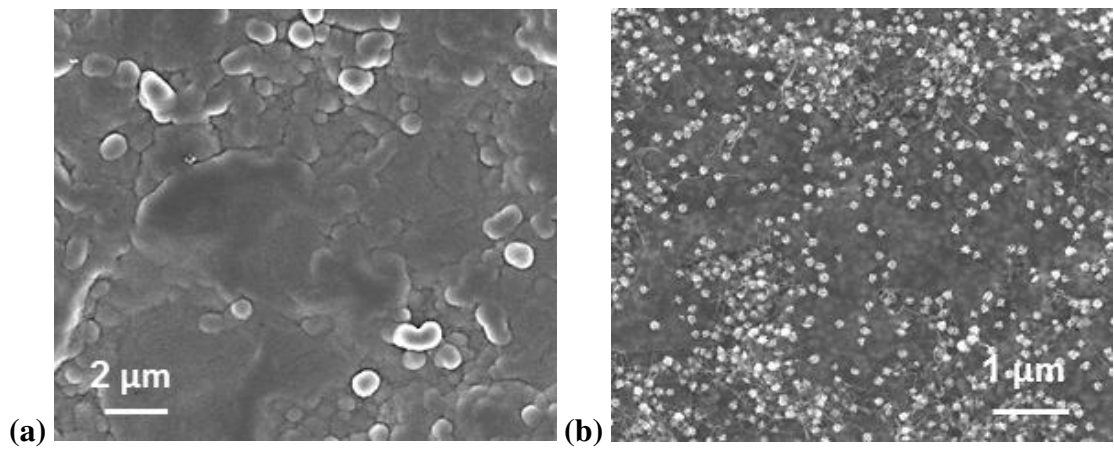


Fig. 3

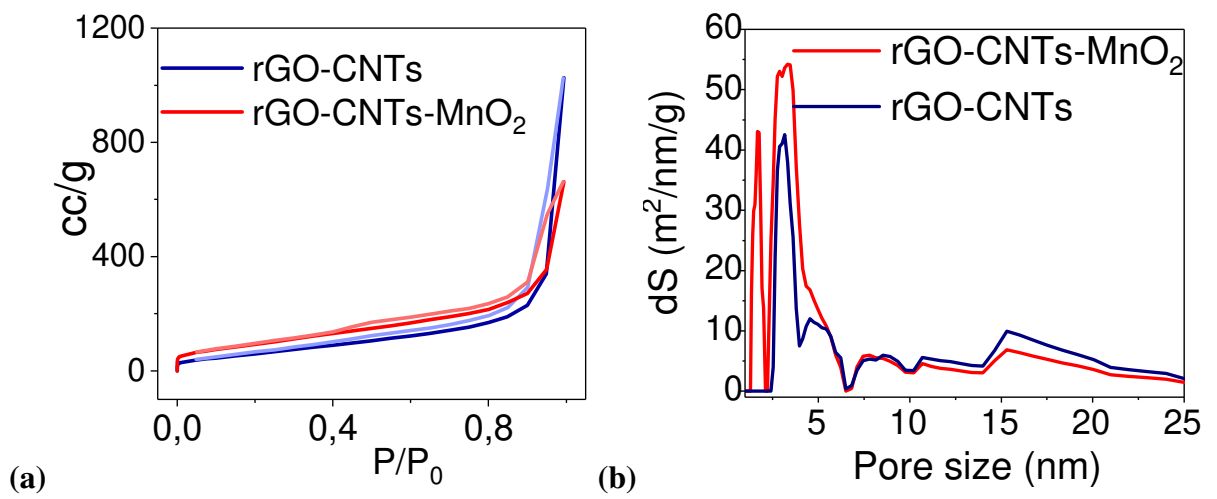


Fig. 4

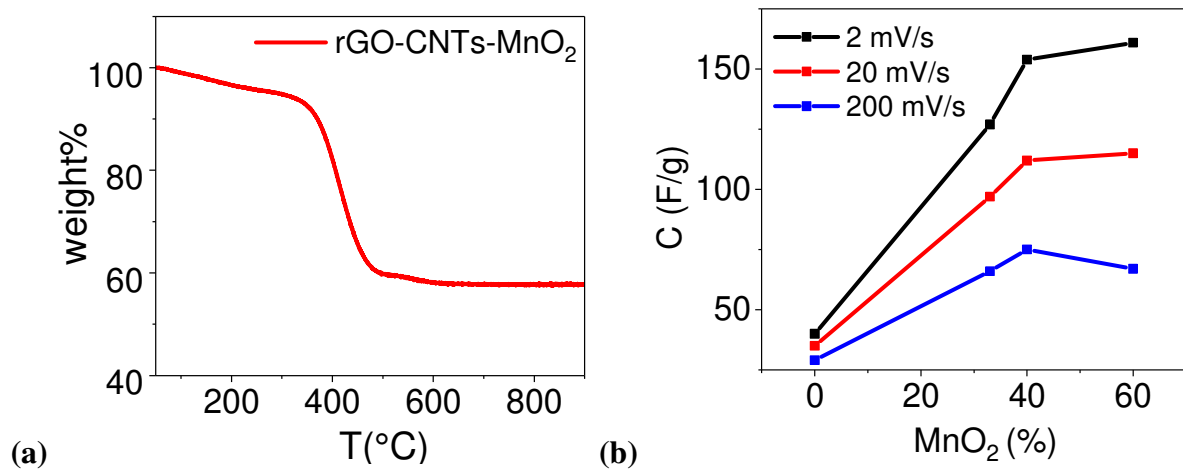


Fig. 5

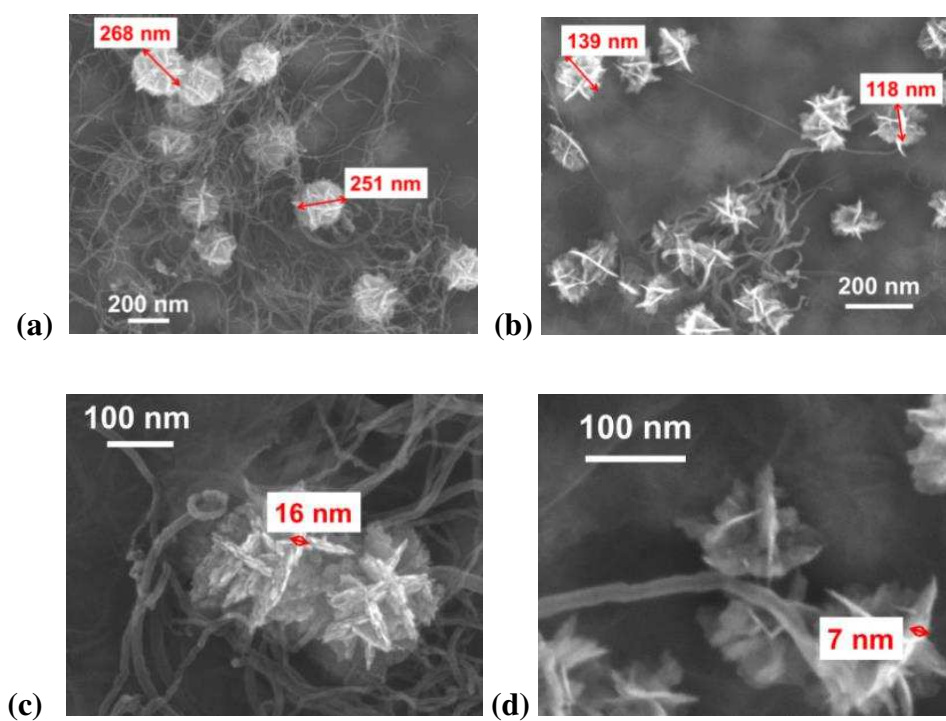


Fig. 6

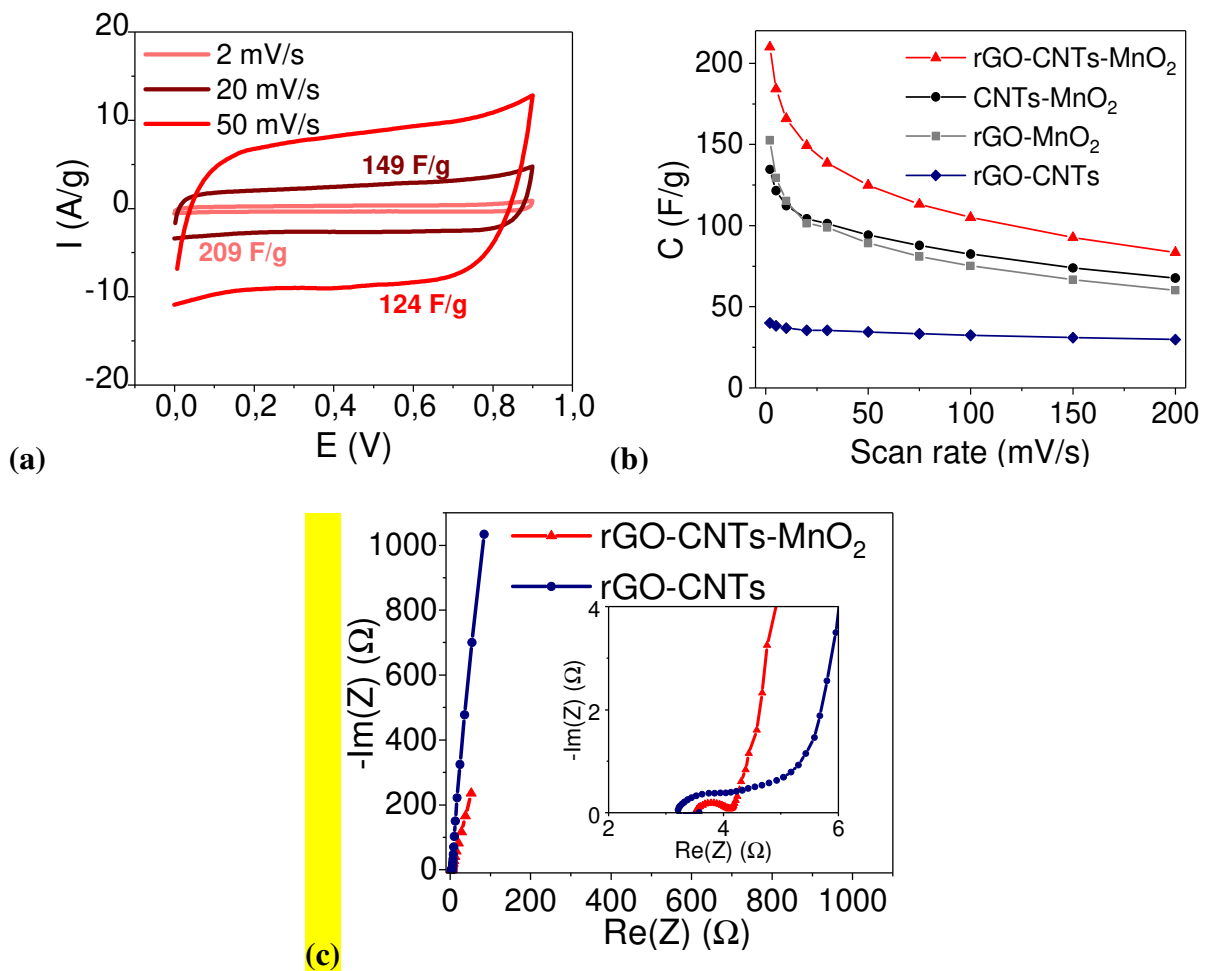


Fig. 7

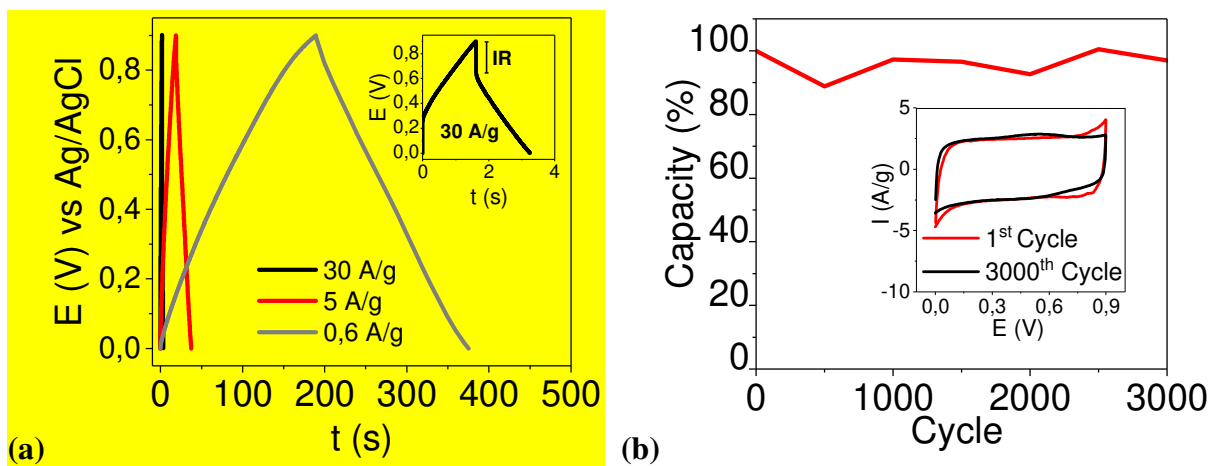


Fig. 8